*Egypt.J.Chem.* **Vol. 63**, No. 5. pp. 1965 - 1976 (2020)

**Egyptian Journal of Chemistry**
**http://ejchem.journals.ekb.eg/**

# Synthesis and Characterization of Low-density Polyethylene Decorated with Ag/rGO Nanocomposite for Packaging Applications

**S. K. Mohamed[1]*, A.A. Abdou[1], A.S.A. Shalaby[2], R.M. Mohsen[3], A.A. F. Zikry[1]**
*[1]Chemistry Department, Faculty of Science, Helwan University, Ain Helwan, Cairo, 11795, Egypt*
*[2]Science and Technology Center of Excellence (STCE), Cairo, Egypt*
*[3]Department of polymers and Pigments, National Research Centre, 33 El Bohouth Street, Dokki-Giza P.O. 12622, Egypt.*

FILMS of low-density polyethylene (LDPE) either blended or coated with different weight percentage (2, 4 and 6 %) of silver-modified reduced graphene oxide (Ag/rGO) have been prepared. Neat LDPE and LDPE blended with Ag/rGO nanocomposite films were prepared by simple casting method while LDPE films coated by Ag/rGO nanocomposite were prepared by applying corona discharge to the as prepared neat LDPE. The prepared samples have been characterized by FTIR, XRD, SEM, EDAX, TEM, DSC and TGA. The mechanical properties and the antimicrobial activities have been examined and compared with that of neat LDPE. From the obtained results, the mechanical properties of polyethylene film were enhanced by blending with very small amount of the as-prepared nanocomposite. The tensile strength of the LDPE film increased up to 60% when added just 4 wt% of Ag/rGO nanocomposite. Coating LDPE by Ag/rGO nanocomposite did not improve the mechanical properties but exhibited antimicrobial activities against *E.Coli* and *S.Aureus*. As the % of Ag/rGO nanocomposite increased in the surface coating layer the antibacterial efficiency increased.

**Keywords:** LDPE, Ag/reduced graphene, Coating, Blending, Antimicrobial.

## Introduction

Plastic packaging is considered as one of the most common industrial applications in our world. In general, plastic materials have chemically inert and nonporous surfaces with low surface tensions which make them suitable for packaging. A modern active packaging system provides protection from three major classes of external influences: chemical, biological, and physical in order to extend product shelf-life, retard deterioration and maintain or increase the quality and safety of food[1]. One of the most common industrial plastics is polyethylene especially low-density polyethylene (LDPE) which is cheap and easy to process. LDPE has very low surface energy [2] and several techniques have been employed to modify its surface properties such as radio-frequency plasma[3], low-pressure plasma[4-6] etching with acid [7] flame treatment [8], irradiation with ionizing and UV radiation [9] and priming [7] and corona discharge [10-12]. The corona discharge is often used for the surface treatment of polymers to enhance its adhesion properties without changing the essential properties of the material [13-16].

Regarding the mechanical properties, it is important to obtain a polymer that sustains the load from handling, processing, transportation, and storing[17]. Active packaging such as antimicrobial packaging is able to destroy microorganisms that contaminate the product or even inhibit its growth rate. The antibacterial packaging films can be made by incorporation and immobilization of antibacterial additives in packaging materials[18-20]. Plastic additives and barrier coatings are the most applicable methods used for the fabrication of active packaging films[21,22] . Many inorganic nanoparticles have

*Corresponding author Tel: +2 01550091550 & Fax: +2 022552468
Email: sahar.kamal@science.helwan.edu.eg & sahar_km2@yahoo.com
Received 23/7/2019; Accepted 29/10/2019
DOI: 10.21608/ejchem.2019.14956.1920

been used to enhance the antibacterial properties of the plastic for packaging such as zinc [23], silver [24], copper [25], manganese, molybdenum, titanium [26] and iron [27].

Recently the researcher focused on graphene and silver nanoparticles due to their intelligent properties. Graphene and its derivatives such as reduced graphene oxide (rGO) have large surface area, very high electron conductivity, very low cytotoxicity, high mechanical strength, and very good chemical and thermal stability[28]. Silver nanoparticles have good stability, broad antibacterial spectrum, and low bacteria resistance [29,30]. The electrical and antimicrobial properties of rGO are improved by impregnating with Ag nanoparticles [31-35]. However, the blending of the aggregations of these nanomaterials with LDPE results in reducing the specific surface area and minimize the antibacterial efficiency of the nanoparticles. The present work aims to prepare new active LDPE film with good mechanical and antibacterial properties for food packaging by blending or coating the polymer with Ag /rGO nanocomposite.

## Experimental

*Materials*

All the chemicals and solvents were used as obtained without further purification. Graphite (99.9%, Fisher Chemical Co), $H_2SO_4$ (95-98%, Marvin), $NaNO_3$ (99,8%, REACHIM), $KMnO_4$ (99,5 %, REACHIM), $H_2O_2$ (30%, Valerus), $AgNO_3$ (Chem-Lab), NaOH (M=40, Valerus), $NaBH_4$ (98 %, Alfa-Aesar), $HSi(OC_2H_5)_3$ (95%, Sigma-Aldrich), low-density polyethylene (LDPE, Sabic 722N), xylene ($C_8H_{10}$, ADWIC), ethyl acetate ($CH_3COOC_2H_5$, ADWIC), and titanium acetyl acetonate ($Ti(C_5H_7O_2)_4$, 99%, Sun-chemical) were used for the preparation of the tested samples.

*Synthesis of graphene oxide GO, Ag/Reduced graphene oxide (Ag/rGO) and LDPE films*

*Synthesis of graphene oxide (GO)*

Graphene oxide was prepared by modified Hummer method [36]. In brief, 0.5 g graphite powder and 0.5 g sodium nitrate were added to 23 ml of sulfuric acid placed in an ice-bath during stirring. To this mixture, 3.0 g potassium permanganate was slowly added and the reaction mixture was stirred for one hour at room temperature then, 100 ml distilled water was added drop wise, the temperature of the reaction raised rapidly to 95 °C. The reaction mixture was diluted by adding 500 ml distilled water then 30 ml $H_2O_2$ (30% v/v) was added so the color change from dark brown to yellow. The product was filtered and washed several times with distilled water to remove the acid residue. The obtained precipitate was dried under vacuum and stored in a desiccator.

*Synthesis of Ag /Reduced graphene oxide (rGO) nanocomposite*

A suspension of prepared GO (540 mg) in 200 ml distilled water was sonicated in a water bath sonicator for 1 hour at 30°C. To this suspension, 1.5 g NaOH and 2.26 g $NaBH_4$ were added gradually and the mixture was stirred for 30 min. A solution of 94.5 mg $AgNO_3$ in 100 ml distilled water was added drop wise to the reaction mixture during stirring at room temperature. The mixture was placed in an ice bath and allowed to settle for 24 hours. The produced precipitate was filtered, washed by distilled water and dried at 80°C for 2 hours. The same steps were done without the addition of $AgNO_3$ to prepare rGO.

*Synthesis of LDPE film*

LDPE film was prepared by simple solvent casting method with optimizing conditions. Briefly, dissolving 1 g of LDPE in 30 ml xylene at 90 °C with stirring then the produced solution was poured in a 15 cm diameter glass petri dish, dried in an air oven at 90°C for 3 h and left at ambient condition for 24 h then kept in a desiccator.

*Synthesis of LDPE /Ag/rGO by blending technique*

Thin films of LDPE/Ag/rGO nanocomposites containing 2, 4, and 6 wt % of Ag/rGO with respect to the LDPE were prepared by blending technique. Initially, the calculated amount of Ag/rGO was dispersed in 20 ml of xylene and 0.5 ml of trimethoxysilane as a dispersant. The mixture was sonicated using water bath sonicator for 2h. and alternatively, 1 g of LDPE was dissolved in 30 ml xylene at 90 °C and stirred for 20 min. The well-dispersed Ag/rGO was added to LDPE solution and stirred for 15 min to ensure good dispersion then the mixture is poured on a 15 cm diameter glass Petri dish. A well-defined film was formed after drying in an oven at 90 °C for 3 h then left at ambient condition for 24 h. The as-prepared film was peeled out to keep in a desiccator. This sample was labeled as LDPE/Ag/rGO-B. Unfortunately the sample of LDPE/Ag/rGO-B (6%) showed aggregation of Ag/rGO and the nanoparticles were not distributed

homogeneously so it was excluded from the study.

*Synthesis of LDPE/Ag/rGO by surface coverage technique*

In this method the dried surface of the prepared neat LDPE film was treated using corona discharge at a power of 4000 W for 1 min, to provide a hydrophilic property to the film's surface for a better attachment of Ag/rGO to the LDPE surface. Definite amount of Ag/rGO (2, 4, and 6 wt% with respect to LDPE) was dispersed in 20 ml of ethyl acetate and 0.5 ml of titanium acetyl acetonate to improve the adhesion of Ag/rGO to the LDPE film and the mixture was sonicated in a water bath sonicator for 2 h. Then, this mixture was sprayed on LDPE film surface and allowed to dry at room temperature. This sample was labeled as LDPE /Ag/rGO-S.

*Characterization*

Fourier transform infrared (FT-IR) spectra were recorded on FT-IR spectroscopy (FT-IR-6100 Jasco, Japan), using KBr pellets in the range of 4000–400 $cm^{-1}$ at room temperature with spectral resolution 4 $cm^{-1}$. X–ray diffraction (XRD) studies were carried out using D8 Advance X-ray diffractometer, Bruker AXS, Germany, with Cu Ka radiation ($\lambda$ = 1.5405 $A^o$) at 40 kV and 60 mA. The surface morphology of the films was studied using Field Emission Scanning Electron Microscope (FE-SEM) (Quanta FEG 250, NL) with disperses X-Rays analysis (EDAX) by AMETEK HoLLand; the sample was coated with gold before SEM testing. High-Resolution Transmission Electron Microscope (HR-TEM) was obtained from a JEOL JEM-2100 Plus (USA) Transmission Electron Microscope. Tensile testing was performed at room temperature on a Zwick Roell dynamometer; tests were carried out at a cross-head speed of 25 mm/min until breaking. The thermal stability of the films was tested using TGA Q500, TA instruments, thermo balance sensitivity 0.1µ g. The weight of the sample (range 5-10 g) was heated from 25 to 600 $^oC$ at a heating rate of 10 $^oC$ $min^{-1}$ under nitrogen, flowing rate of 50 ml $min^{-1}$. The glass transition of the films was explored using Differential scanning calorimeter (DSC) in a TA Instruments Q2000 model equipped with a RCS90 cooling unit. The heat flow and the heat capacity of the DSC instrument were calibrated at 2 $^oC$ $min^{-1}$ using indium and sapphire standards respectively. Sample weight 5-10 mg was placed in aluminum pans with an ordinary aluminum lid.

*Antimicrobial activity*

The antimicrobial activities of nanocomposite and prepared samples were investigated against Gram-negative bacteria *Escherichia coli* (*E. coli*) and Gram-positive bacteria *Staphylococcus aureus* (*S. aureus*) and different type of fungi such as *Aspergillus flavus* (*A. flavus*) and *Candida albicans (C. albicans)* by using agar well diffusion method and the flask shake method [37].

## Results and Discussion

*XRD analysis*

Fig (1) illustrates the XRD patterns of the as prepared samples of GO, rGO, and Ag/rGO. As shown, the GO exhibits a sharp peak at 2Θ of 10.5° and (001) diffraction plane. This peak is attributed to the oxygenated functional groups as hydroxyl and epoxide groups which formed at the boundary of the graphite sheets between the plane and carboxylic acid, and results in the exfoliation of graphitic layers[38]. For rGO, as a result of reduction reaction, oxygenated functional groups disappeared [39] and a broad peak at $26.6^0$ 2Θ appears which was attributed to the (002) plane with an interlayer spacing of 0.359 nm where the rGO layers were exfoliated[40]. Ag/rGO sample shows the characteristic peaks of Ag at the 2Θ of $38.1^o$ (111), $44.3^o$ (200), $64.4^o$ (220), $77.4^o$ (311) and $81.4^o$ (222) which revealed the presence of cubic crystal of silver[41],(JCPDS File No. 01-087-0597). The average crystallite size of the silver nanoparticles inside the Ag/rGO sample was calculated by Scherrer's equation as ≈13 nm.

Fig.2. shows the XRD patterns of the prepared neat LDPE, LDPE/Ag/rGO-B and LDPE/Ag/rGO-S films with 6 wt% Ag/rGO. As shown in the fig, neat LDPE showed two peaks at 2Θ value of 21.56° and 23.84°, which are assigned to the (110) and (200) lattice planes of the material. These diffraction peaks did not change as a result of blending or surface coverage of with Ag/rGO. This observation confirm that the polymer structure did not change by blending or coating with Ag/rGO nanocomposite This was attributed to the small amount of the fully exfoliated Ag/rGO nanocomposite inside or on the surface of the LDPE film [42].

*FTIR analysis*

FTIR spectra of Ag/rGO, neat LDPE, LDPE /Ag/rGO-B and LDPE /Ag/rGO-S films are explored in Fig.3. As shown, in the case of Ag/ rGO, the characteristic band at 1630 $cm^{-1}$ and 2920 $cm^{-1}$ related to the aromatic C=C and $CH_2$ asymmetric stretching respectively. The absence of the absorption bands at 1734, 1228, 1084 $cm^{-1}$, of C=O, C-O-C, alkoxy C-O stretching vibration indicates the disappearance of surface oxygen containing groups which suggests the successful reduction of GO [43]. However, the small absorption bands at 3430, 2350 and 1027 $cm^{-1}$, indicating the presence of some –OH and –COOH groups in rGO sample which suggests that the GO particles were reduced partially [44,45]. The spectrum of neat LDPE showed absorption bands at 2942 $cm^{-1}$ and 2866 $cm^{-1}$ of (CH) stretching vibration as well as absorption bands at 722 $cm^{-1}$ and 1464 $cm^{-1}$ belong to the skeletal vibrations of $CH_2$. LDPE/Ag/rGO-B and LDPE/Ag/rGO-S showed additional absorption bands at 469 $cm^{-1}$ related to Ag banding and oxygen functional group from rGO. The absorption band at 1100 $cm^{-1}$ intensified which could be attributed to the physical binding of C–C–H group with Ag/rGO nanoparticles [46,47]. Therefore, the FT-IR spectra

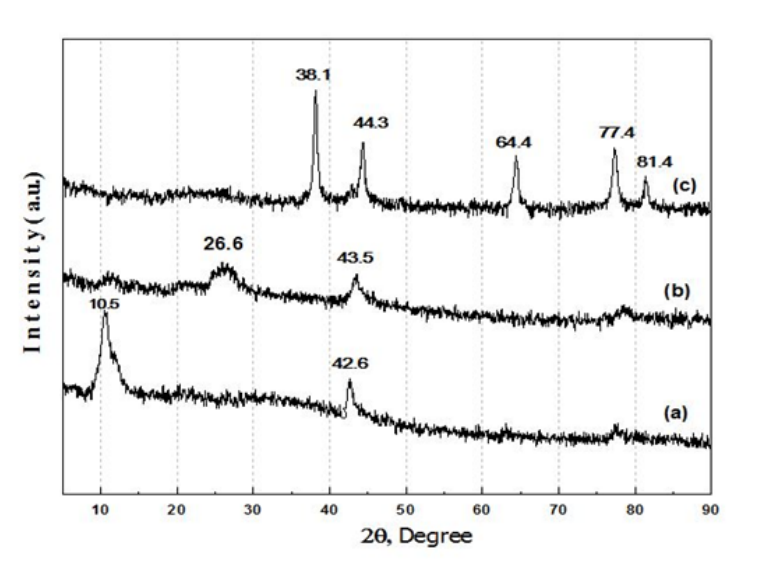


**Fig.1. XRD patterns of (a) GO, (b) rGO and (c) Ag/ rGO nanocomposite**

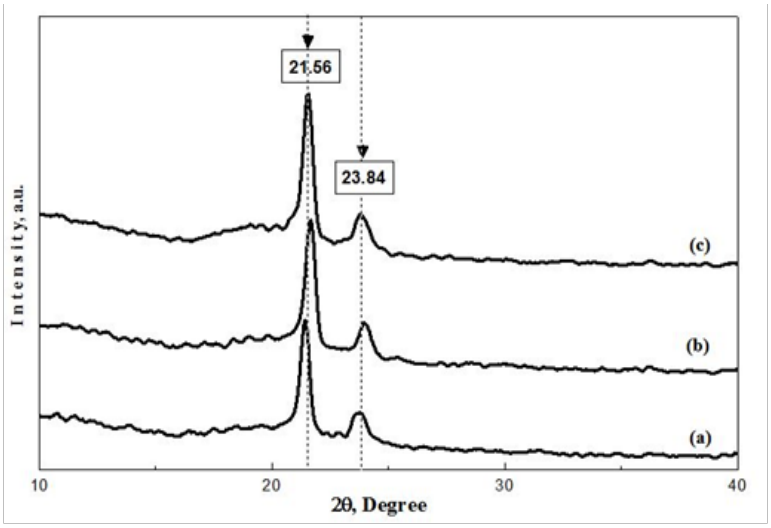


**Fig.2. XRD patterns of (a)neat LDPE (b) LDPE /Ag/rGO-B and (c) LDPE /Ag/rGO-S film.**

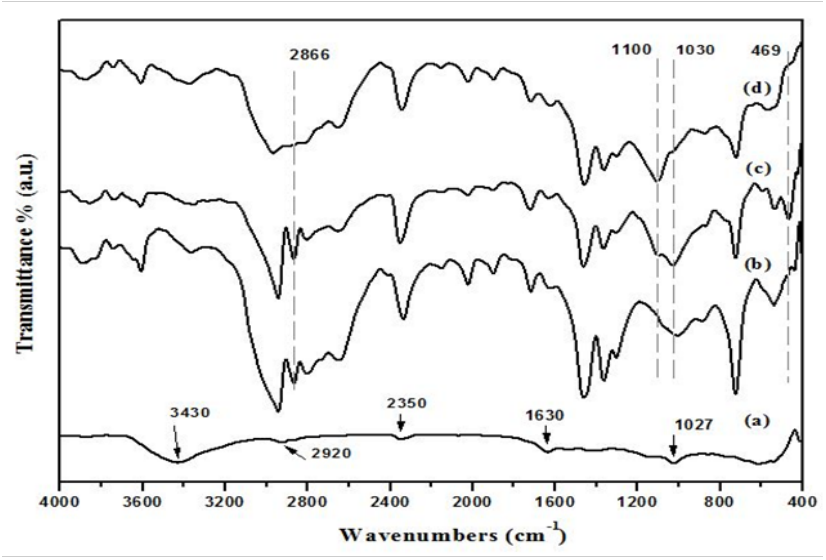


**Fig.3. FTIR spectra of (a) Ag/rGO, (b) neat LDPE, (c) LDPE/Ag/rGO-B and (d) LDPE/Ag/rGO-S samples.**

certified the existence of physical interaction forces such as van-der Waals forces between the chain of LDPE and Ag/rGO nanocomposite.

*SEM analysis*

Fig. 4 shows the SEM images of the prepared samples. The morphology of the as prepared Ag/rGO nanocomposite showed rGO sheets decorated with randomly distributed silver clusters and to confirm the reduction of Ag ions into Ag metallic particles, EDAX analysis was carried out as shown in Fig 4 (A, B). LDPE /Ag/rGO-B film with 4% Ag/rGO exhibits amorphous-like surface with bright small aggregates which related to the Ag nanoparticles inside the randomly distributed Ag/rGO nanocomposite blended with LDPE as shown in Fig. 4(C). LDPE /Ag/rGO-S film with 4% Ag/rGO showed a cracked layer of Ag/rGO on the polymeric substrate as shown in Fig. 4(D).

*TEM analysis*

Fig. 5 shows TEM images of prepared samples. Fig. 5 (a & b) of Ag/rGO shows the uniform distribution of Ag nanoparticles on rGO sheets where Ag nanoparticles (black dots) show polydispersed spherical shape with diameter ranges from 4 to 21 nm. It was noticed that the layered structure of the rGO is wrinkled where many Ag nanoparticles are uniformly anchored on its surface. The image of LDPE /Ag/rGO-B film with 4% Ag/rGO (Fig 4C) shows uniformly dispersed spherical Ag nanoparticles on rGO sheet within the polymeric matrix. Fig 4D shows the image of LDPE /Ag/rGO-B film with 4% Ag/rGO. As shown, Ag nanoparticles are dispersed on the rGO sheets that cover the surface of the polymeric LDPE film.

*TGA analysis*

The thermal stability of neat LDPE films and LDPE/Ag/rGO-B with 2 and 4 wt% of Ag/rGO was studied using TGA analysis and the results are explored in Fig.6. The thermal degradation of the samples showed two stages, the first stage starts at 200 $^{o}$C up to 400 $^{o}$C. In this stage, neat LDPE showed only 4% weight loss while LDPE/Ag/rGO-B with 2 and 4 wt % of Ag/rGO showed weight loss of 4.5 and 10.3 %, respectively. This was attributed to the thermal degradation of rGO where the oxygen-containing functional groups on rGO produce CO, $CO_2$ and $H_2O$ vapors. Furthermore, the high thermal conductivity of the Ag/rGO nanocomposite in addition to a small amount of internal oxygen enhances the burning of the carbon inside the LDPE sheet. The second stage of thermal degradation started around 400$^{o}$C where samples dramatically degraded due to the burning of the skeletal carbon of LDPE chains. At 500 $^{o}$C neat LDPE, LDPE/Ag/rGO-B (2%) and LDPE/Ag/rGO-B (4%) exhibited weight loss of 99.6, 96.7 and 95.0 wt% respectively. The difference in the residual ratio was attributed to the inorganic Ag particles.

*DSC analysis*

DSC analysis was performed to investigate the melting point ($T_m$) and crystallization temperature of neat LDPE films and LDPE /Ag/rGO-B with 2

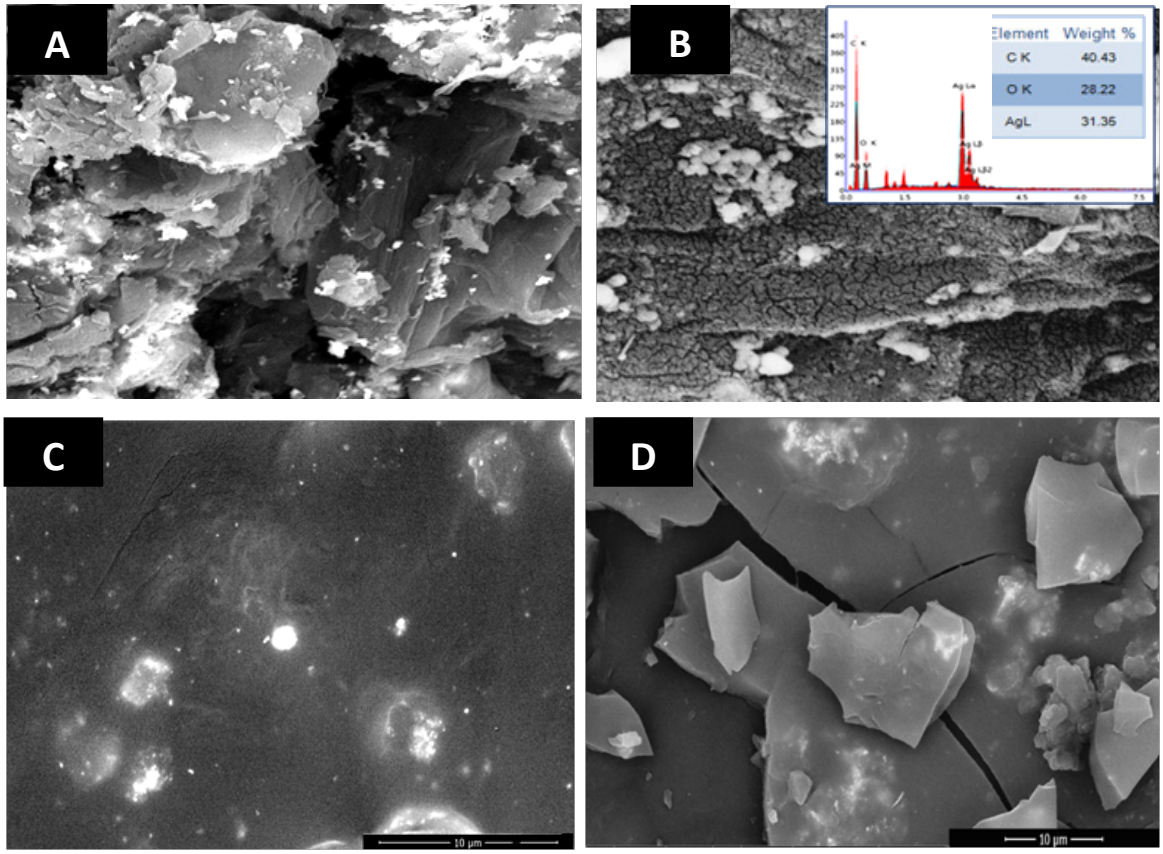


**Fig.4. SEM images of (A, B) Ag/rGO nanocomposite powder, (C) LDPE/Ag/rGO-B film surface and (D) LDPE/Ag/rGO-S film surface.**

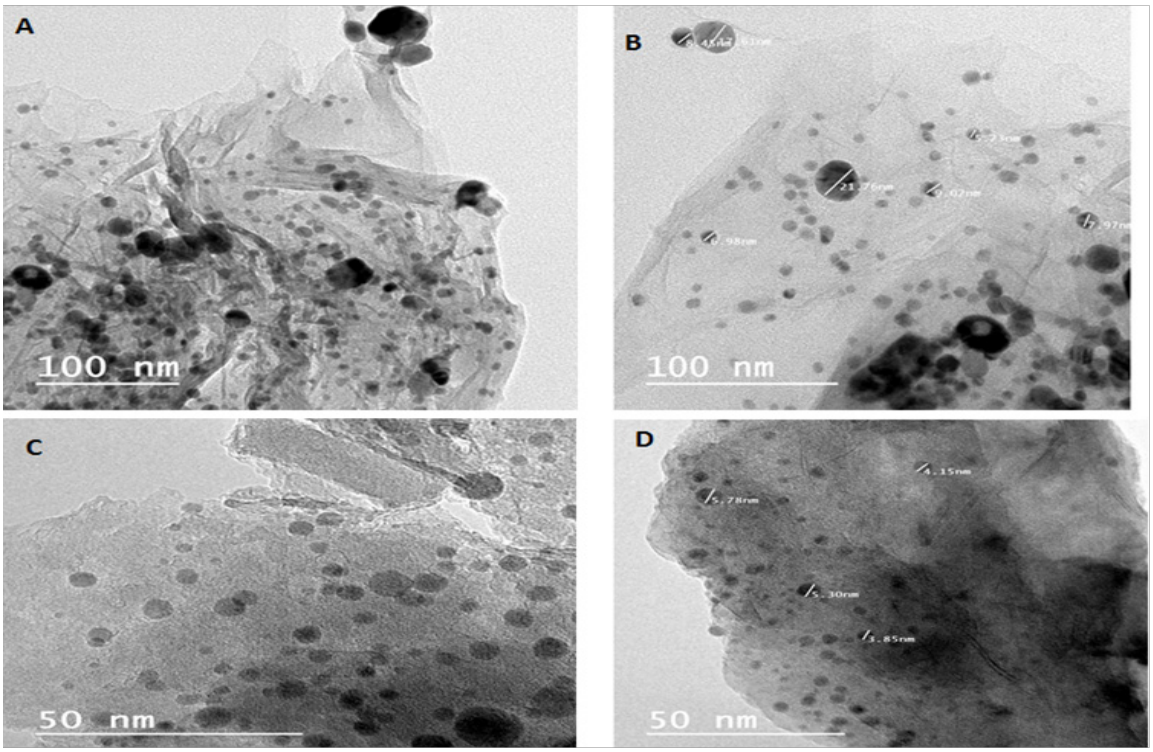


**Fig.5. TEM images of (a, b) Ag/rGO nanocomposite, (c) LDPE/Ag/rGO-B and (d) LDPE/Ag/rGO-S film.**

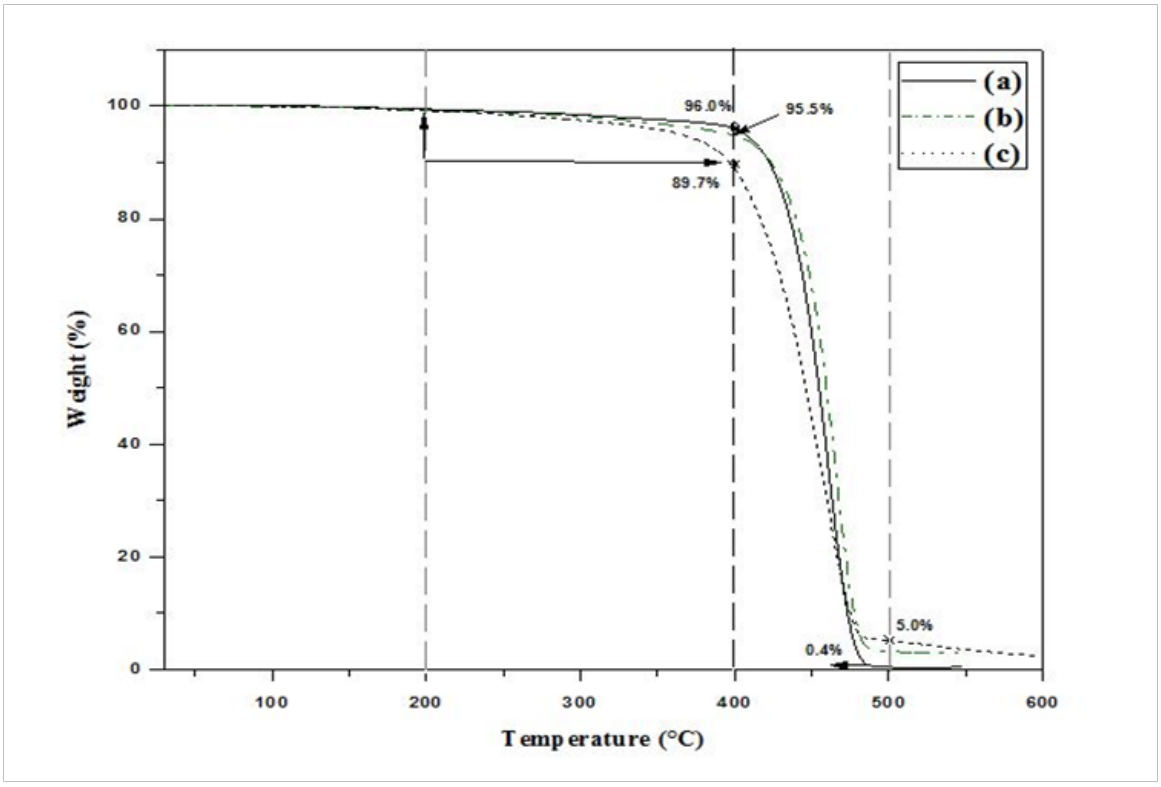


**Fig.6. TGA analysis of (a) neat LDPE, (b) LDPE/Ag/rGO-B (2 wt%) and (c) LDPE/Ag/rGO-B(4 wt%) films.**

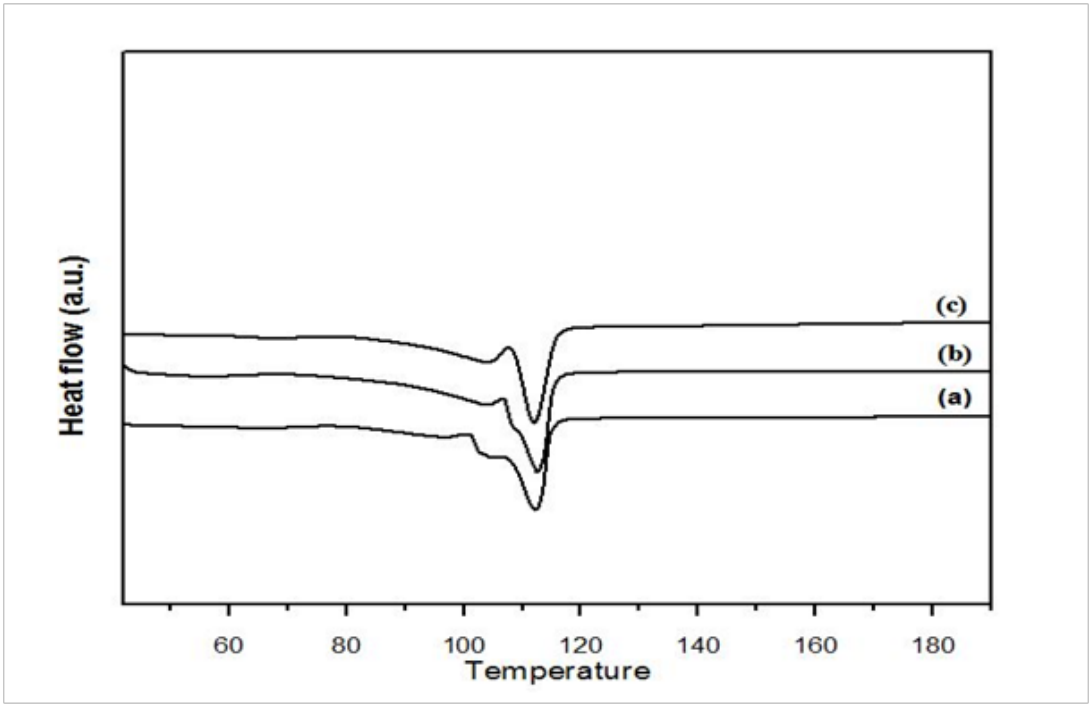


**Fig.7. DSC of (a) neat LDPE, (b) LDPE/Ag/rGO-B (2 wt%) and (c) LDPE/Ag/rGO-B (4 wt%).**

and 4 wt% of Ag/rGO. The results of the second cycle heating curve from-20 to 200°C with a heating rate 10 °C $min^{-1}$ and nitrogen flow of 50 ml $min^{-1}$ are presented in Fig.7 and Table 1.

As shown in the figure no significant differences in the melting temperature of all samples were observed. The enthalpy and crystallinity of samples were decreased as Ag/rGO (%) increased (Table 1). This was attributed to the good dispersion of Ag/rGO in the polymeric matrix which restricts the crystallization of the polymer chains. The enthalpy change of LDPE / Ag/rGO-B was also relatively smaller than that of neat LDPE [48].

*Mechanical properties*

The mechanical properties of as prepared samples were detected by measuring the tensile strength (TS) and elongation at break (EAB) as shown in Fig.8 (a & b). According to the results of show significant increase in the tensile stress and drop in the elongation at break in the LDPE /Ag/rGO-B films compared with the neat LDPE films. The tensile properties of LDPE are strongly varied by blending with the Ag/rGO incorporation where the tensile strength increased by 33% and 60% as a result of blending LDPE with 2 and 4 % Ag/rGO respectively. The enhancement in the tensile strength is revealed to the physical association of the polymer chains with the rGO layers which would restrict the motion of the chains by fixing them in their vicinity. Usually, The enhancement in the tensile strength of the polymers as a result of filler additions are accompanied with the well dispersion and good interfacial interaction among the polymer and the filler [49]. LDPE/Ag/rGO-S samples showed similar tensile strength (TS) and elongation at break (EAB) for neat LDPE.

*Antibacterial activity*

The antibacterial activity of the Ag/rGO nanocomposite was explored by using agar well diffusion method against different types of bacteria (*E.Coli* & *S.Aureus*) and results showed that the growth inhibition zones in the bacteria plates of *E.Coli* and *S.Aureus* were 15 mm and 14 mm respectively as shown in Fig.9 (a, b).

Ag/rGO nanocomposites exhibit antibacterial activity through double effect mechanism where the bacteria are captured by rGO nanosheets which biologically isolate them and prevent their proliferation. Ag nanoparticles, decorating rGO surface, penetrate the cell wall membrane and destroy the bacteria [50]. Such activity of the nanocomposite can restrict the microbial growth via capturing-killing mechanism in a certain region [51].

All LDPE/Ag/rGO-B samples did not show any antimicrobial activity which was attributed to the capsulation of the Ag/rGO nanocomposite inside the hydrophobic polymer (LDPE) which prevent their destructive effect. However, in case of plastic sheet failure for any reason, the microbes can't penetrate the packaging plastic sheet containing Ag/rGO nanocomposite. In the case of LDPE/Ag/rGO-S samples, the antimicrobial activities are clearly detected. Since Agar well diffusion for the coating of a LDPE film can't distinguish bactericidal and bacteriostatic effects, so the samples were measured by the dynamic shake flask tests regarding to the percentages of

**TABLE1. Thermal parameters of neat LDPE and LDPE/Ag/rGO-B as detected from second heating cycle DSC curve .**

| Sample | Melt Onset Temperature (°C) | Melt Peak Temperature (°C) | Enthalpy (J/g) | Crystallinity (%) |
|---|---|---|---|---|
| **Neat LDPE** | 106.56 | 112.33 | 59.63 | 20.8 |
| **LDPE /Ag/rGO-B (2 wt%)** | 106.98 | 112.51 | 44.99 | 15.7 |
| **LDPE /Ag/rGO-B (4 wt%)** | 108.60 | 112.06 | 37.18 | 13 |

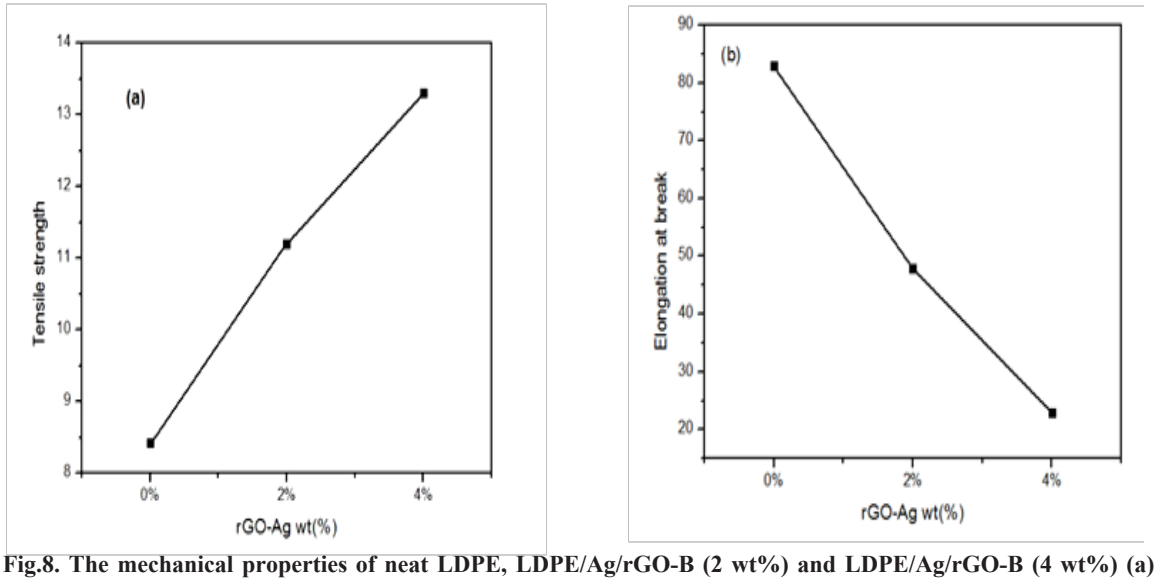


**Fig.8. The mechanical properties of neat LDPE, LDPE/Ag/rGO-B (2 wt%) and LDPE/Ag/rGO-B (4 wt%) (a) Tensile strength (b) Elongation at break.**

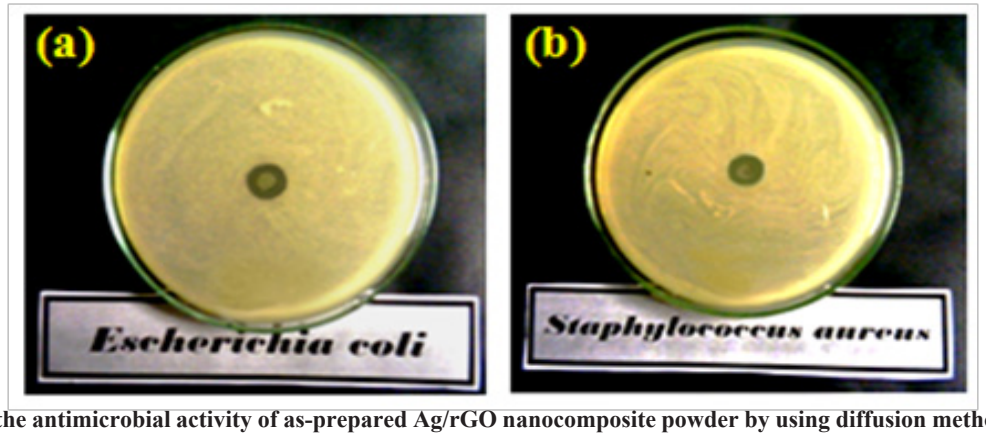


**Fig.9. the antimicrobial activity of as-prepared Ag/rGO nanocomposite powder by using diffusion method against different types of bacteria (a) E.Coli (b) S.Aureus .**

**TABLE 2. Antibacterial properties of coated of LDPE film by the flask shake method.**

| Sample | *Staphylococcus Aureus* ($G^+$) [R%] | *Escherichia Coli* ($G^-$) [R%] |
|---|---|---|
| **LDPE** | 0 | 0 |
| **LDPE /Ag/rGO-S (2 wt%)** | 0 | 0 |
| **LDPE /Ag/rGO-S (4 wt%)** | 10.31 | 2.57 |
| **LDPE /Ag/rGO-S (6 wt%)** | 14.23 | 2.97 |

* R% bacterial growth reduction percentage

reduction obtained against the growth of *E.Coli* and *S.Aureus* and the results are shown in Table 2.

Surface coating by 2 wt% of Ag/rGO didn't produce a significant reduction, while LDPE /Ag/rGO-S (4 wt %) exhibits a percentage of reduction of 10.31% for *S.Aureus* and 2.57% for *E.Coli*. Growth reduction value was enhanced to 14.23% for *S.Aureus* and 2.97% for *E. coli* by coating the film with 6 wt% of Ag/rGO.

## Conclusion

Active plastic packaging films of LDPE treated with Ag/rGO nanocomposite were successfully prepared by using solvent casting method and surface coating methods by the aid of corona discharge technique. The analysis characterized the prepared Ag/rGO nanocomposite and confirmed its antimicrobial activities against $G^+$ and $G^-$ bacteria. The nanocomposite additives enhanced the mechanical and antimicrobial properties of LDPE films. LDPE/Ag/rGO-B showed enhanced mechanical properties while LDPE/Ag/rGO-S showed better antimicrobial and antifungal efficiency. Results proved that Ag/rGO nanocomposite is a promising nano-additive for production of antibacterial films for packaging applications.

## References


1. Marsh K., Bugusu B., Food packaging roles, materials, and environmental issues. J Food Sci. 72 (3), R39-R55 (2007).
2. Markgraf, D.A., Corona Treatment: An Overview, Coextrusion Conference Proceedings, TAPPI PRESS, Atlanta, p.85 (1986).
3. Ilić V., Šaponjić Z., Vodnik V., Molina R., Dimitrijević S., Jovančić P., Nedeljković J., Radetić M., Antifungal efficiency of corona pretreated polyester and polyamide fabrics loaded with Ag nanoparticles. J Mater Sci. 44 (15), 3983-3990 (2009).
4. Nobile M.A.del., Cannarsi M., Altieri C., Sinigaglia M., Favia P., Iacoviello G., d'Agostino R.,EffectofAg□containingnano□compositeactive packaging system on survival of Alicyclobacillus acidoterrestris. J Food Sci. 69 (8), E379-E383 (2004).
5. Jiang H., Manolache S., Wong A.C.L., Denes F.S., Plasma□enhanced deposition of silver nanoparticles onto polymer and metal surfaces for the generation of antimicrobial characteristics. J Appl Polym Sci. 93 (3), 1411-1422 (2004).
6. Dhayal M., Alexander M.R., Bradley J.W., The surface chemistry resulting from low-pressure plasma treatment of polystyrene: The effect of residual vessel bound oxygen. Appl Surf Sci. 252 (22), 7957-7963 (2006).
7. Sadeghnejad A., Aroujalian A., Raisi A., Fazel S., Antibacterial nano silver coating on the surface of polyethylene films using corona discharge. Surf Coat Technol. 245,1-8 (2014).
8. Strobel M., Lyons C.S., An essay on contact angle measurements. Plasma Process Polym. 8 (1), 8-13 (2011).
9. Park S-J., Jin J-S., Effect of corona discharge treatment on the dyeability of low-density polyethylene film. J Colloid Interface Sci. 236 (1), 155-160 (2001).
10. Jones V., Strobel M., Prokosch M.J., Development of poly (propylene) surface topography during corona treatment. Plasma Process Polym. 2 (7), 547-553 (2005).
11. Hirvikorpi T., Vähä-Nissi M., Harlin A., Marles J., Miikkulainen V., Karppinen M., Effect of corona pre-treatment on the performance of gas barrier layers applied by atomic layer deposition onto polymer-coated paper board. Appl Surf Sci. 257 (3), 736-740 (2010).
12. Gadri R., Roth J.R., Montie T.C., Kelly-Wintenberg K., Tsai P., Helfritch D., Feldman P., Sherman D., Karakaya F., Chen Z., Sterilization and plasma processing of room temperature surfaces with a one atmosphere uniform glow discharge plasma (OAUGDP). Surf Coatings Technol. 131 (1-3), 528-541 (2000).
13. Desai S.M., Singh R.P., Surface modification of polyethylene. In: Albertsson, A.-C. (ed.) Long Term Properties of Polyolefins. Springer, Berlin, 231-294 (2004).
14. Novák I., Pollak V., Chodak I., Study of surface properties of polyolefins modified by corona discharge plasma. Plasma Process Polym. 3 (4□5), 355-364 (2006).
15. Zhu L-P., Zhu B-K., Xu L., Feng Y-X., Liu F., Xu Y-Y., Corona-induced graft polymerization for surface modification of porous polyethersulfone membranes. Appl Surf Sci. 253 (14), 6052-6059 (2007).
16. Friedrich J., Wigant L., Unger W., Lippitz A.,

Wittrich H., Corona spark and combined UV and ozone modification of polymer films. Surf coatings Technol. 98 (1-3), 879-885 (1998).

17. Fortunati E., Multifuntional films, blends, and nanocomposites based on chitosan: Use in antimicrobial packaging. In J. Barros-Velazquez (Ed.), Antimicrobial food packaging (1st ed): Academic Press, 467-477 (2016).

18. Scannell A.G., Hill C., Ross R.P., Marx S., Hartmeier W., Elke G., Arendt K., Development of bioactive food packaging materials using immobilised bacteriocins, Lacticin and Nisaplin. Int J Food Microbiol. 60 (2-3), 241-249 (2000).

19. Appendini P., Hotchkiss J.H., Immobilization of lysozyme on food contact polymers as potential antimicrobial films. Packag Technol Sci An Int J. 10 (5), 271-279 (1997).

20. Appendini P., Hotchkiss J.H., Review of antimicrobial food packaging. Innov Food Sci Emerg Technol. 3 (2), 113-126 (2002).

21. Natrajan N., Sheldon B.W., Efficacy of nisin-coated polymer films to inactivate Salmonella typhimurium on fresh broiler skin. J Food Prot. 63 (9),1189-1196 (2000).

22. Sánchez□Valdes S., Ortega□Ortiz H., Ramos□de Valle L.F., Medellín□Rodríguez F.J., Guedea□Miranda R., Mechanical and antimicrobial properties of multilayer films with a polyethylene/silver nanocomposite layer. J Appl Polym Sci. 111 (2), 953-962 (2009).

23. Kaczmarek M.T., Jastrząb R., Hołderna-Kędzia E., Radecka-Paryzek W., Self-assembled synthesis, characterization and antimicrobial activity of zinc (II) salicylaldimine complexes. Inorganica Chim Acta. 362 (9), 3127-3133 (2009).

24. Kim J.S., Kuk E., Yu K.N., Kim J.H., Park S.J., Lee H.J., Kim S.H., Park Y.K., Park Y.H., Hwang C.Y., Kim Y.K., Lee Y.S., Jeong D.H., Cho M.H., Antimicrobial effects of silver nanoparticles. Nanomedicine. 3 (1), 95-101 (2007).

25. Ren G., Hu D., Cheng E.W.C., Vargas-Reus M.A., Reip P., Allaker R.P., Characterisation of copper oxide nanoparticles for antimicrobial applications. Int J Antimicrob Agents. 33 (6), 587-590 (2009).

26. Nomiya K., Onodera K., Tsukagoshi K., Shimada K., Yoshizawa A., Itoyanagi T., Sugie A., Tsuruta S., Sato R., Kasuga N., Syntheses, structures and antimicrobial activities of various metal complexes of hinokitiol. Inorganica Chim Acta. 362 (1), 43-55 (2009).

27. Richards A.D., Rodger A., Hannon M.J., Bolhuis A., Antimicrobial activity of an iron triple helicate. Int J Antimicrob Agents. 33 (5), 469-472 (2009).

28. Liu L., Bai H., Liu J., Sun D.D., Multifunctional graphene oxide-TiO2-Ag nanocomposites for high performance water disinfection and decontamination under solar irradiation. J Hazard Mater. 261, 214-223 (2013).

29. Liu F., Guo N., Chen C., Meng X., Shao X., Microwave synthesis Ag/reduced graphene oxide composites and enhanced antibacterial performance. Mater Res Innov. 20 (7), 512-517 (2016).

30. Tian T., Shi X., Cheng L., Luo Y., Dong Z., Gong H., Xu L., Zhong Z., Peng R., Liu Z., Graphene-based nanocomposite as an effective, multifunctional, and recyclable antibacterial agent. *ACS Appl Mater Interfaces*. **6** (11), 8542-8548 (2014).

31. Movahed S.K., Dabiri M., Bazgir A., Palladium nanoparticle decorated high nitrogen-doped graphene with high catalytic activity for Suzuki–Miyaura and Ullmann-type coupling reactions in aqueous media. *Appl Catal A Gen*. **488**, 265-274 (2014).

32. Martínez-Orozco R.D., Rosu H.C., Lee S-W., Rodríguez-González V., Understanding the adsorptive and photoactivity properties of Ag-graphene oxide nanocomposites. *J Hazard Mater*. **263**, 52-60 (2013).

33. Wang D., Yang J., Li X., Geng D., Li R., Cai M., Sham T-K., Sun X., Layer by layer assembly of sandwiched graphene/$SnO_2$ nanorod/carbon nanostructures with ultrahigh lithium ion storage properties. *Energy Environ Sci*. **6** (10), 2900-2906 (2013).

34. Namvari M., Namazi H., Clicking graphene oxide and $Fe_3O_4$ nanoparticles together: an efficient adsorbent to remove dyes from aqueous solutions. *Int J Environ Sci Technol*. **11** (6), 1527-1536 (2014).

35. Ghasemi S., Esfandiar A., Setayesh S.R., Habibi-Yangjeh A., Gholami M.R., Synthesis and characterization of $TiO_2$–graphene nanocomposites modified with noble metals as a photocatalyst for degradation of pollutants. *Appl*

*Catal A Gen*. **462**, 82-90 (2013).

36. .Sinitskii A., Sun Z., Slesarev A., Alemany L., Lu W., Tour J., Improved synthesis of graphene oxide. *ACS Nano.* **4**, 4806-4814 (2010).

37. Bauer A.W., Kirby W.M.M., Sherris J.C., Turck M., Antibiotic susceptibility testing by a standardized single disk method. *Am J Clin Pathol*. **45** (4), 493-496 (1966).

38. Bielawski C.W., Dreyer D.R., Park S., Ruoff R.S., The chemistry of grapheme oxide. *Chem Soc Rev*. **39** (1), 228-240 (2010).

39. Gao W., Alemany L.B., Ci L., Ajayan P.M., New insights into the structure and reduction of graphite oxide. *Nat Chem*. **1** (5), 403 (2009).

40. Rajaura R.S., Srivastava S., Sharma V., Sharma P.K., Lal C., Singh M., Palsania H.S., Vijay Y.K., Role of interlayer spacing and functional group on the hydrogen storage properties of graphene oxide and reduced graphene oxide. *Int J Hydrogen Energy*. **41** (22), 9454-9461 (2016).

41. Weiwei W., Wenfang W., Xiaoli C., Yucheng W., Lingshu D., Synthesis and characterization of Ag/ graphene nano-composite. *Rare Met Mater Eng*. **44** (9), 2138-2142 (2015).

42. Lei H., Liu Z., He C., Zhang S-C., Liu Y-Q., Hua C-J., Li X-M., Li F., Chen C-M., Caiad R., Graphene enhanced low-density polyethylene by pretreatment and melt compounding. *RSC Adv*. **6** (103), 101492-101500 (2016).

43. Fan B., Guo H., Shi J., Shi C., Jai Y., Wang H., Chen D., Yang Y., Lu H., Xu H., Zhang R., Facile one-pot preparation of silver/reduced graphene oxide nanocomposite for cancer photodynamic and photothermal therapy. *J Nanosci Nanotechnol*. **16** (7), 7049-7054 (2016).

44. Yang X., Xu M., Qiu W., Chen X., Deng M., Zhang J., Iwai H., Watanabe E., Chen H., Graphene uniformly decorated with gold nanodots: in situ synthesis, enhanced dispersibility and applications. *J Mater Chem*. **21** (22), 8096-8103 (2011).

45. Moon I.K., Lee J., Ruoff R.S., Lee H., Reduced graphene oxide by chemical graphitization. *Nat Commun*. **1**, 73 (2010).

46. Gupta K., Jana P.C., Meikap A.K., Optical and electrical transport properties of polyaniline–silver nanocomposite. *Synth Met*. **160** (13-14), 1566-1573.(2010).

47. Shameli K., Bin-Ahmad M., Jazayeri S.D., Sedaghat S., Shabanzadeh P., Jahanirian H., Mahdavi M., Abdollahi Y., Synthesis and characterization of polyethylene glycol mediated silver nanoparticles by the green method. *Int J Mol Sci*. **13** (6), 6639-6650 (2012).

48. Chang M-K., Mechanical properties and thermal stability of low-density polyethylene grafted maleic anhydride / montmorillonite nanocomposites. *J Ind Eng Chem*. **27**, 6-11 (2014).

49. Usman A., Hussain Z., Riaz A., Khan A.N., Enhanced mechanical, thermal and antimicrobial properties of poly (vinyl alcohol)/ graphene oxide /starch/silver nanocomposites films. *Carbohydr Polym*. **153**, 592-599 (2016).

50. Zhang M., Zhao Y., Yan L., Peltier R., Hui W., Yao X., Cui Y., Chen X., Sun H., Wang Z., Interfacial engineering of bimetallic Ag/Pt nanoparticles on reduced graphene oxide matrix for enhanced antimicrobial activity. *ACS Appl Mater Interfaces*. **8** (13), 8834-8840 (2016).

51. Ganguly S, Das P, Bose M, Das TK., Mondal S., Das A.K., Das N.C., Sonochemical green reduction to prepare Ag nanoparticles decorated graphene sheets for catalytic performance and antibacterial application. *Ultrason Sonochem*. **39**, 577-588 (2017).